

A MULTIWAVELENGTH STUDY OF THE EXTREME AGN J2310-437

D.M. WORRALL^{1,2}, M. BIRKINSHAW^{1,2}, R. A. REMILLARD³, A. PRESTWICH², W. H. TUCKER²,
H. TANANBAUM²,

Printed July 27th 1998. To appear in The Astrophysical Journal

ABSTRACT

We present new X-ray, radio, and optical data for the unusual galaxy/cluster system J2310-437. Our results confirm the presence of an active nucleus, and suggest an interpretation as an anomalous BL Lac object of bulk relativistic Doppler factor < 2 , with an optically deficient radio-to-X-ray spectrum. The radio, optical, and soft X-ray flux densities could lie along a single power-law function, lacking the curvature typical of BL Lac objects. Compared with other known sources that may have comparable multifrequency spectra, J2310-437 is the most extreme. Its low isotropic optical/UV radiation is consistent with the intensity of external photons governing the electron spectral break through Compton cooling; in this source the external photon density would be too low to produce a spectral break below the X-ray.

1. INTRODUCTION

The galaxy/cluster system J2310-437 is unusual. CCD images and spectroscopy identified the *Einstein* X-ray source E2307-44 (B1950 coordinates) with a galaxy of $V = 16.05 \pm 0.02$ mag and $z = 0.0886$ at the center of a cluster of Abell richness class 0 (Tucker, Tananbaum & Remillard 1995). ROSAT PSPC observations showed X-ray extent (Tananbaum et al. 1997). However, while the 0.5-2.5 keV luminosity⁴ of $\sim 7.5 \times 10^{43}$ ergs s⁻¹ would make J2310-437 one of the most luminous known cluster X-ray sources for its richness class (cf Briel & Henry 1993), a plausible but non-unique interpretation of the PSPC data was a combination of cluster and AGN emission. Tananbaum et al. (1997) favored associating about 80% of the X-rays with an AGN, noting the $\sim 20''$ positional coincidence of the galaxy with the 61 mJy radio source J2310-437 from the PMN 4.85 GHz survey (Griffith & Wright 1993; Condon, Griffith & Wright 1993). However, they pointed out the lack of evidence for an AGN in the optical, where the spectrum is typical of a normal elliptical galaxy, devoid of emission lines. The radio and X-ray strength combined with the upper limit on optical continuum from the putative AGN component would place it as an extreme BL Lac object.

In this paper we present ROSAT HRI observations which verify the compact nature of much of the X-ray emission. Radio imaging and polarization measurements with the Australia Telescope Compact Array (ATCA) confirm the identification of the X-ray emitting galaxy with the radio source. We present a new optical spectrum from which we derive improved upper limits to an optical AGN component. Finally, we discuss the classification of this extreme source, its relation to other AGN populations, and the process that might be responsible for its multiwavelength properties.

2. ROSAT HRI X-RAY OBSERVATIONS

If indeed $\sim 80\%$ of the X-rays detected with the PSPC were from an AGN, the better spatial resolution of the HRI was expected to reveal a core of bright unresolved emission in our

50 ks exposure. The ROSAT scheduling algorithm caused the HRI observations to be carried out in two unequal observing periods roughly 6 months apart; details are given in Table 1. Our analysis was performed with the IRAF/PROS. Spatial analysis also used generalized software (Birkinshaw 1994; Worrall & Birkinshaw 1994) for fitting radial profiles to combinations of models convolved with instrument Point Response Functions (PRFs).

The ROSAT HRI data for the region in the vicinity of J2310-437 are shown smoothed and contoured in Figure 1. The data from 1995 give radially symmetric contours whereas the 1996 data show clear ellipticity with the major axis running roughly east-west. The two data sets were taken at different spacecraft roll angles, and the apparent difference in source shape is undoubtedly because the 1996 data are more affected by residual errors in the aspect corrections applied to the photons (Appendix A). The impact on our analysis is that we use only the (higher-quality) 1995 data to probe the spatial distribution of X-rays associated with J2310-437; unfortunately these data represent just less than 20% of the total HRI exposure. Both data sets have been used to search for X-ray variability.

2.1. Spatial Decomposition

Aside from the effects of the aspect-correction residual errors in the 1996 HRI data, there is no obvious extended X-ray emission associated with J2310-437; instead a bright central component is seen, and two fainter sources are detected within a radius of 3 arcmin (Fig. 2). The 1995 data give an excellent fit to the nominal PRF of David et al. (1996), as seen in Figure 3.

The HRI data constrain the models which Tananbaum et al. (1997) fit to the ROSAT PSPC data. The PSPC data give an *acceptable* fit to a single component β model, appropriate for gas in hydrostatic equilibrium⁵. However, applying the corresponding best-fit model parameters to the 1995 HRI data gives $\chi_{\min}^2 = 169$ for 17 degrees of freedom, as compared with $\chi_{\min}^2 = 14$ for the fit to a point source (18 degrees of freedom).

The PSPC data give an *unacceptable* fit to unresolved emission alone, and so why is there no resolved emission evident

¹Department of Physics, University of Bristol, U.K.

²Harvard-Smithsonian Center for Astrophysics, Cambridge, MA 02138

³Massachusetts Institute of Technology, Cambridge, MA 02139

⁴We use $H_0 = 50$ km s⁻¹ Mpc⁻¹, $q_0 = 0$ throughout. At the redshift of J2310-437, 1 arcsec corresponds to 2.27 kpc.

⁵The β -model notation adopted here (e.g., Sarazin 1986, and see Table 4) relates to the King-model formalism in Tananbaum et al. (1997) via $p = 3\beta - 0.5$.

TABLE 1
ROSAT HRI OBSERVATIONS OF J2310-437.

Dates	Number of intervals	Total Livetime (ks)	Nominal Roll Angle
Nov 22 - 30, 1995	6	7.437	36°
May 1 - Jun 4, 1996	23	31.435	-141°

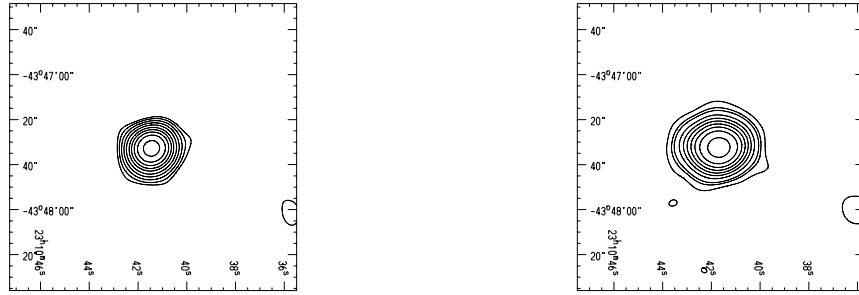


FIG. 1.— HRI data from 1995 (left) and 1996 (right). Pixels are 0.5×0.5 arcsec square and the plots show a 256×256 pixel region centered on J2310-427. The data have been smoothed with a Gaussian of $\sigma = 4$ arcsec. In each case the lowest contour corresponds to a value which should occur only in four pixels of the map by chance (i.e., 3.8σ significance), as determined using a method appropriate for Poisson statistics (Hardcastle et al. 1998b). For the 1995 data (which fit a point source: Fig. 3) the maximum is 0.91 cts/pixel and contours are at 0.011, 0.018, 0.03, 0.05, 0.08, 0.13, 0.19, 0.28, 0.42, and 0.7. For the 1996 data the maximum is 2.14 cts/pixel and contours are at 0.018, 0.04, 0.06, 0.12, 0.2, 0.3, 0.44, 0.64, 0.92, and 1.6.

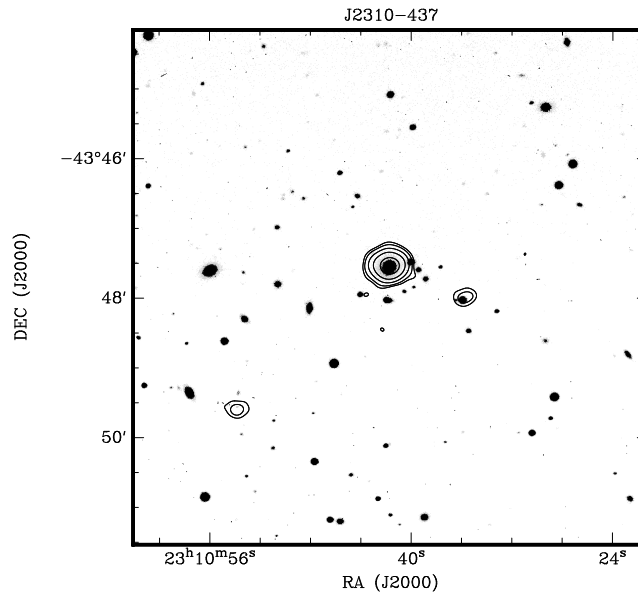


FIG. 2.— HRI X-ray contours from the (longer) 1996 observation superimposed on an R-band CTIO 1.5 m telescope CCD image; the contour threshold is determined as for Figure 1. Two X-ray sources in addition to J2310-437 are seen; the one to the SW may be associated with a galaxy, whereas that to the SE may be associated with a faint object apparent in the I-band image of Tananbaum et al. (1997). Neither of these additional X-ray sources was detected in the radio in our ATCA observations.

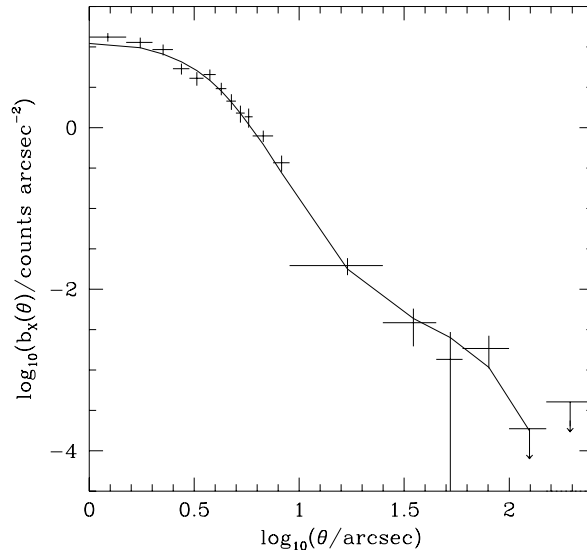


FIG. 3.— The observed HRI radial profile from November 1995 (net counts and 1σ uncertainties plotted as crosses) gives an excellent fit to a point source characterized by the nominal PRF of David et al. (1996); $\chi^2 = 13.7$ for 18 degrees of freedom. Background, as measured in a source-centered annulus of radii 2.5 to 4 arcmin, has been subtracted from the data, and the PRF is normalized to the net counts in the profile.

in the HRI data? We have extended the PSPC model fitting beyond that described in Tananbaum et al. (1997) in order to examine two-component fits (β -model plus unresolved emission) in which the relative normalizations of the two components are allowed to vary. Results are shown in Figure 4. The best-fit model has $\beta = 2/3$ and core radius $\theta_{\text{cx}} = 25$ arcsec, with roughly 80% of the counts in the unresolved component. However, larger β and θ_{cx} are allowed within 90% confidence limits, and then the emission in the unresolved component becomes closer to 90%.

We have fitted the HRI radial profile to point-like plus resolved emission, where the combination of parameters describing the resolved emission (including normalization) is constrained by the PSPC fits (Fig. 4). We allow the normalization of the point-like component to be a free parameter, since this emission might plausibly have varied in intensity between the epoch of the PSPC observations (Nov. 1993) and that of the HRI. Our spectral conversions use the Galactic column density with a power law of energy index $\alpha = 1.43$ ($f_\nu \propto \nu^{-\alpha}$) for the point-like emission and a Raymond-Smith spectrum of $kT = 1.18$ keV (50% cosmic abundances) for the β -model components (Tananbaum et al. 1997). Although the two-component model giving the best fit to the PSPC data is a relatively poor fit to the HRI data, there are models within the 90% confidence range for the PSPC which are acceptable (Table 2). The constraint on extended emission from the HRI data places a lower limit of $\sim 0.36 \mu\text{Jy}$ on the 1 keV flux density of the unresolved emission measured with the PSPC, with a preferred value of $0.4 \mu\text{Jy}$. We adopt $\beta = 2/3$, $\theta_{\text{cx}} = 55$ arcsec as the new best-fit β -model parameters.

2.2. X-ray Light Curve

Table 2 gives the ratio of the 1 keV flux densities for the point component in the HRI and PSPC fits. Although no value

is inconsistent with unity at high confidence (save the $\beta = 2/3$, $\theta_{\text{cx}} = 6$ arcsec model, which can be ruled out on the basis of χ^2), and values are closer to unity in cases where the fits are more acceptable, there is a suggestion that the flux density increased by about 10% between the PSPC (Nov. 1993) and HRI (Nov. 1995) observations. Any hardening of the spectrum with time would increase the ratio; for example, hardening to $\alpha = 0.65$ (closer to the extrapolated radio to X-ray spectral index, see later), means values in column 5 of Table 2 should be multiplied by a factor of 1.4. The HRI observations indicate no significant change in intensity between Nov. 1995 ($0.078 \pm 0.0034 \text{ cts s}^{-1}$) and May 1996 ($0.071 \pm 0.002 \text{ cts s}^{-1}$) and no significant intra-month variability. However, the complexity of the source and our rather imprecise knowledge of the extended structure and source spectrum conservatively suggest that variability of the point component by as much as 50% over a timescale of a few years cannot be ruled out.

3. ATCA RADIO OBSERVATIONS

We observed J2310-437 with the CSIRO/ATNF Australia Telescope Compact Array (ATCA) for 13 hours (including setup and calibration) between UT 1997 January 29th 22:30 and January 30th 11:30. The array was in the 6A configuration, giving baselines from 0.34 to 6 km. All six antennas were on line for most of the time. The observations were made in four frequency bands (Table 3), with half the time at L and S bands, and half at C and X. Observing intervals were interleaved to give full hour-angle coverage and no large gaps in the uv-plane. Heavy rain and thick cloud necessitated phase and gain calibrations every 12 minutes. Secondary calibrations used the nearby quasar PKS 2311-452, while the primary flux-density calibration is based on observations of PKS 1934-638 at the beginning and middle of the 13-hour run. 32 frequency channels were used for each band; 16 of these are independent, but one (chan-

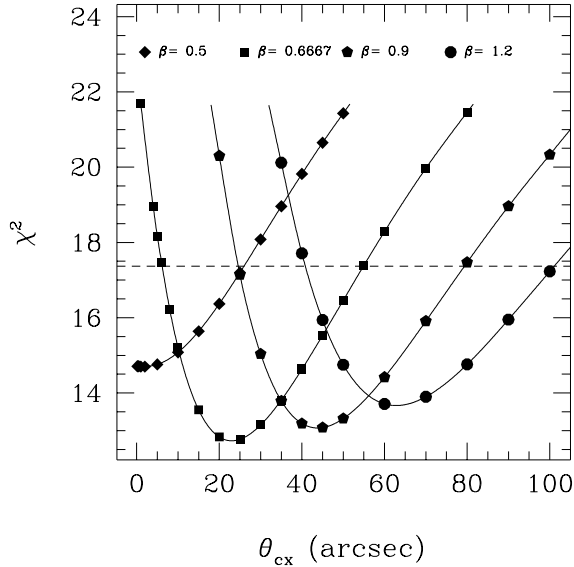


FIG. 4.— χ^2 vs core radius, θ_{cx} for a fit of the ROSAT PSPC radial profile (1172 net counts) in 14 bins out to a radius of 210 arcsec with a β -model plus point source. The β -model parameters for the best fit are $\beta = 2/3$ and $\theta_{\text{cx}} = 25$ arcsec. The dashed line is at $\chi_{\text{min}}^2 + 4.6$, corresponding to 90% confidence for two interesting parameters. As an extension to the work of Tananbaum et al. (1997), the fraction of counts in the point source (within the extraction radius), f , has been fitted rather than fixed at 0.8. The maximum permitted fraction (f_{max}) for any β is at the largest permitted θ_{cx} for that β . We find that f_{max} depends negligibly on the value of β and is ~ 0.9 at 90% confidence. f_{min} for a given β corresponds to the smallest permitted θ_{cx} for that β . For example, $f_{\text{min}} = 0.5$ for $\beta = 2/3$, $\theta_{\text{cx}} = 6$ arcsec, and $f_{\text{min}} = 0.76$ for $\beta = 1.2$, $\theta_{\text{cx}} = 40$ arcsec.

TABLE 2
HRI RADIAL FITS TO A PSPC-NORMALIZED β MODEL PLUS A POINT SOURCE.

β	θ_{cx} (arcsec)	t_{cool} (yr) ^a	$f_{1 \text{ keV, AGN}}$ (μJy) ^b	$\left(\frac{\text{HRI}}{\text{PSPC}}\right)_{\text{AGN}}$ ^c	χ^2 for 17 dof
0.5	2	3.2×10^8	0.33 ± 0.014	1.19 ± 0.08	25.5
0.5	25	1.3×10^{10}	0.39 ± 0.014	1.09 ± 0.065	17.0
2/3	6	5.8×10^8	0.22 ± 0.014	1.51 ± 0.13	88.0
2/3	25	7.4×10^9	0.37 ± 0.014	1.13 ± 0.07	26.6 ^d
2/3	55	2.7×10^{10}	0.40 ± 0.014	1.09 ± 0.065	16.7 ^e
0.9	25	4.6×10^9	0.33 ± 0.014	1.21 ± 0.08	50.9
0.9	80	3.6×10^{10}	0.40 ± 0.014	1.08 ± 0.065	16.9
1.2	100	4.3×10^{10}	0.40 ± 0.014	1.08 ± 0.065	17.4

^aAverage cooling time within θ_{cx} . These values should be compared with a Hubble time of $\sim 2 \times 10^{10}$ yr.

^b1 keV flux density for the unresolved component from the PSPC fit, corrected for the fact that only 96% of the PSPC counts lie within a source-centered circle of radius 3.5 arcmin.

^cRatio of normalization of the unresolved emission in the HRI and PSPC fits, corrected for the response of the instruments assuming a power-law spectrum with $\alpha = 1.43$ and Galactic absorption.

^dBest-fit case for the PSPC data.

^eAdopted as giving new best-fit parameter values.

NOTE.—Figure 4 shows goodness of fits to the PSPC data.

nel 4) was removed because of self interference, and the two end channels were removed because of low signal strength. 10-second integrations were used for all observations at all bands. The data were calibrated, mapped, and self-calibrated using the ATNF's Miriad software package. Final mapping and polarization analysis used AIPS, with weighting schemes chosen to maximize signal-to-noise or to permit the best spectral-index measurements.

3.1. Radio Images and Polarization

Figure 5 shows contour maps of the processed data for each frequency band with polarization E vectors superimposed. The maps are affected by uv-sampling and frequency; the L-band image provides our best information about large-scale structure and the X-band measures the core and inner jet-structure only.

3.1.1. X Band

The image shows one-sided extended emission to the SE with 16 ± 3 mJy of diffuse emission extending about 10 arcsec at a position angle of 150° . This jet appears to come out from the core at a position angle of about 130° . Core polarization of about 2% is seen, with the magnetic field aligned perpendicular to the jet. Polarization in the jet is detected at low signal to noise and appears to peak at $\sim 15\%$ about 2 arcsec SE of the nucleus, still with the inferred magnetic field perpendicular to the jet.

3.1.2. C Band

The total flux in our measurements is 42 ± 4 mJy. Since the PMN survey measured 61 mJy (Griffith & Wright 1993), about 20 mJy of C-band diffuse emission should be present on scale sizes greater than 20 arcsec, which is the largest scale to which the 6A array is sensitive. It is also possible that a variable core contributes to the discrepancy. The diffuse structure and jet are one sided and resemble the X-band in structure and polarization. There is no significant Faraday rotation present between X and C bands.

3.1.3. S Band

The image shows two-sided structure with some evidence of tails curving back to the N and ESE. The polarization structure in the core is particularly striking. A small rotation of the plane of polarization, about 15 degrees, is seen relative to the E vectors at C band.

3.1.4. L Band

The curvature of the two-sided tail structure is most evident at this frequency. The total measured flux density is about 99 mJy, and the extent of the L-band image is roughly that of the cluster-related PSPC X-rays. The spectral index between the S and L bands in the SE and NE lobes is $\alpha \sim 0.8$ ($f_\nu \propto \nu^{-\alpha}$), in the normal range for optically-thin synchrotron emission. The position angle of the jet to the SE is similar to that in the inner region at X-band, suggesting bending from a position angle of $\sim 130^\circ$ to $\sim 150^\circ$ and back to $\sim 130^\circ$ with increasing distance from the core. The E vectors in the core are rotated by about 50 degrees with respect to those at S band, and the polarized fraction peaks at about 30%, to the NW of the core. The Faraday rotation measure, which is about -25 radians m^{-2} (varying by ~ 10 radians m^{-2} over the inner part of the source), could arise entirely from gas and fields in our Galaxy.

3.2. The Radio Core

The radio core lies at $\alpha = 23^{\text{h}} 10^{\text{m}} 41^{\text{s}}.76 \pm 0.01$, $\delta = -43^\circ 47' 34''.3 \pm 0.3$ (J2000). The flux densities (Table 3) imply a flat spectrum, with a component of the emission becoming optically thin between the C and S bands. While the position confirms the association between the radio emission, the optical galaxy, and the X-ray source, there are remaining small discrepancies. The galaxy centroid determined from the Southern Sky Survey, as digitized by the Space Telescope Science Institute, agrees in right ascension but is 1.6 arcsec north in declination. The most likely explanation is an error in the calibration of the optical reference frame for this part of the sky. The centroid of the HRI position agrees to within an arcsecond with that from the digitized sky survey; on the one hand this is surprising because the HRI aspect-correction uncertainties can result in centroids which are in error by several arcseconds, but on the other hand the closer agreement to the optical centroid than to the radio position may reflect the fact that X-ray positions are determined with respect to the optical reference frame rather than the radio. The X-ray centroid for the lower-resolution PSPC data (Tananbaum et al. 1997) is 3.5 arcsec to the south of the radio core.

3.3. The Overall Radio Structure

At X- and C-band the radio structure is predominantly one-sided. Since at lower frequencies the structure is clearly two-sided, a possible interpretation is that the source is a (slightly wiggly) twin jet, where the SE side experiences greater Doppler boosting towards the observer. The data allow us to place limits on the jet to counter-jet ratio, R , of > 3 from the X-band map (with $R \sim 3.5$ on $2''$ scale), and > 8 on $5''$ scales from the C-band map. At S- and L-band the resolution is too low to provide useful information.

It is hard to classify this source by comparison with other radio sources seen in poor clusters. However, in section 5.2.1 we note that at least one radio source, the X-ray selected BL Lac object 0548-322, has a similar morphology. If the bending in J2310-437 which is measured at L-band continues at lower surface brightness, the source power and structure are somewhat reminiscent of narrow-angle tail (NAT) sources such as 3C 83.1 B, in which the jets are bent back to become approximately parallel. However, such sources are usually associated with non-dominant cluster galaxies, with the bending attributed to motion of the host galaxy through the intra-cluster medium. Wide-angle tail (WAT) sources are more often seen in the centers of clusters. The prototypical WAT is 3C 465 in Abell 2634, but WATs also occur in poor clusters, such as the source 1919+479 (Pinkey, Burns & Hill 1994). The bending of WATs is often interpreted as due to galaxy mergers. WAT sources are typically larger than 500 kpc in extent, whereas the L-band emission we measure in J2310-437 spreads only over about 300 kpc. Also the jets in WATs tend to show hot-spots at the position of bending, rather than the smooth fall-off in intensity seen in J2310-437. J2310-437 is more reminiscent of low power radio galaxies such as 3C 449 or 3C 31, but unlike them exhibits a severely bent outer structure. More sensitive X-ray measurements of the cluster environment are needed before we can say if this bending can be explained as a buoyancy effect or interaction with the hot X-ray emitting gas.

4. CTIO OPTICAL SPECTRUM

Our earlier optical spectrum of J2310-437 (Tucker et al. 1995) did not cover $\text{H}\alpha$ or the Ca II break, but both re-

TABLE 3
RADIO-CORE FLUX DENSITIES AT THE FOUR OBSERVING FREQUENCIES.

Band	Frequency (MHz)	f_{core} (mJy)
L	1384	27.7 ± 2.0
S	2368	27.9 ± 0.6
C	4800	20.6 ± 0.5
X	8640	20.9 ± 0.3

NOTE.—All bands were 112 MHz wide, centered on the reported frequency, with an 8 MHz “notch” for a missing channel

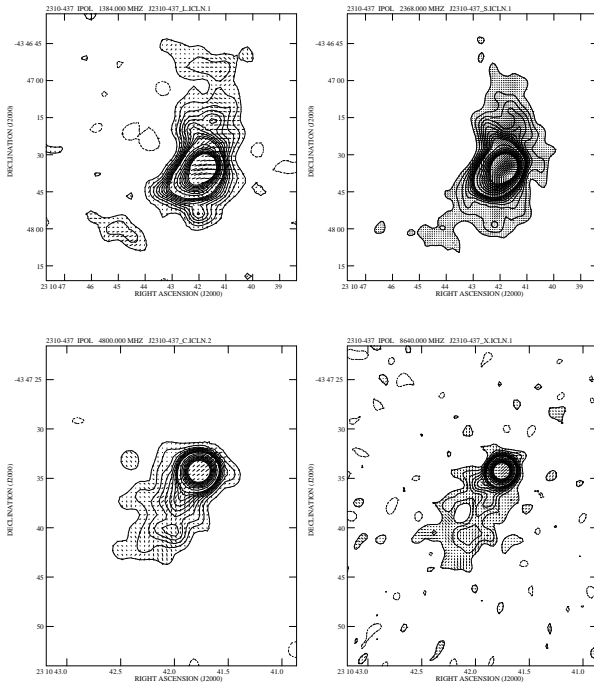


FIG. 5.— L-band (top left), S-band (top right), C-band (bottom left) and X-band (bottom right) radio maps of J2310-437 with polarization E vectors (length proportional to polarized flux) superimposed. Note scale change between upper and lower figures. The restoring Gaussian beams have a FWHM of $6.5''$ (L-band and S-band), $2''$ (C-band) and $1.5''$ (X-band). Contours are at 0.2, 0.4, 0.6, 0.8, 1, 1.2, 1.4, 1.6, 1.8, 2, 3, 4, 5, 6, 7, 8, 9, 10 mJy, with -0.2 mJy shown dashed. The maps show a transverse magnetic field following the line of the jet and significant radio polarization in the core. The signal to noise of the polarization is low within the lowest three contours of each map.

gions can provide evidence for nuclear activity. Consequently, new observations were performed with the CTIO 1.5 meter telescope on 1996 May 15. We used the Cassegrain spectrograph with the Loral 1K CCD. The wavelength range of 3800 – 7230 Å was sampled with 8 Å resolution (FWHM), using a slit width of 3 arcsec. The exposure time was 1500 s during clear sky conditions, and the subsequent target was a flux calibration standard that was observed at a similar value of the air mass (1.20). Spectral reductions and calibrations were performed using IRAF. We deliberately limited the extraction aperture to a window of ± 1.5 arcsec, thereby sampling only the $3'' \times 3''$ core of the galaxy. The result is shown in Figure 6. There is no H α emission line, at an upper limit of 6.0×10^{-16} ergs cm $^{-2}$ s $^{-1}$. For comparison purposes, we also extracted a spectrum from a source-centered $12'' \times 3''$ region.

The blue end of the $3'' \times 3''$ spectrum (Fig. 6) shows normal absorption features, including the Ca II H and K lines and the g band, redshifted by $z = 0.0886$. Following Dressler & Shectman (1987) we quantify the size of the Ca II break as the fractional drop in flux (f_ν units) between the 4050-4250 Å and 3750-3950 Å galaxy rest-frame bands. The values found (0.46 ± 0.02 for the $3'' \times 3''$ spectrum and 0.47 ± 0.02 for the $12'' \times 3''$ spectrum) are both in the normal range for elliptical galaxies.

Since there is no evidence of H α emission, we derive an upper limit for the blue emission from any AGN nucleus by calculating the maximum continuum that can be added to the $3'' \times 3''$ spectrum before the Ca II break is diluted to 0.40, the value proposed by Marchã et al. (1996) as borderline between galaxies with and without an AGN continuum, and a value $\sim 3\sigma$ away from our results. A convenient model for the continuum source is provided by H1722+119 (Brissenden et al. 1990), which is an X-ray selected BL Lac object (XBL) with no evidence for a visible host galaxy. The optical continuum of H1722+119 is well fit by a single power law with $f_\lambda \propto \lambda^{-0.12}$, corresponding to $f_\nu \propto \nu^{-1.88}$. In using this relatively steep (i.e., red) spectrum rather than the average value of $f_\nu \propto \nu^{-0.65}$ found (with large dispersion) for multiple observations of 10 XBLs by Falomo, Scarpa & Bersanelli (1994), we are being conservative by tending to maximize the allowed nonthermal contribution to the spectrum of J2310-437 at the Ca II break. After converting to the observed frame, for frequencies close to the Ca II break we find a maximum BL Lac flux density of $f_\lambda = 1.4 \times 10^{-16}(\lambda/\text{Å})^{-0.12}$ ergs cm $^{-2}$ s $^{-1}$ Å $^{-1}$; $f_\nu = 2.5 \times 10^{29}(\nu/\text{Hz})^{-1.88}$ μJy .

Evidence that an AGN optical continuum may lurk at a level close to our limit comes from comparing our results with Caccianiga & Maccacaro (1997)'s recent spectrum taken using the ESO 3.6 m telescope with a 1.5 arcsec slit. From an extraction region of $0.6'' \times 1.5''$ (Maccacaro 1997; private communication), containing less galaxy light than our $3'' \times 3''$ spectrum, they find a Ca II break of 0.38 ± 0.04 compared with our value of 0.46 ± 0.02 . Although the values are consistent to within 2σ , they suggest that a central continuum may dilute the break. When the spectral extraction region excludes the inner $1.8'' \times 1.5''$ of the galaxy, Caccianiga & Maccacaro (1997) find a contrast of 0.47 ± 0.05 , in good agreement with our results. A detailed comparison of the allowed level of nonthermal continuum is not possible, since the Caccianiga & Maccacaro spectrum has no absolute flux calibration, and different slit widths and extraction apertures are used. However, their measurement is consistent with roughly equal AGN and elliptical galaxy contributions at ~ 4300 Å (observed frame) if the elliptical galaxy

has a normal Ca II break of 0.6. This result may be in agreement with our upper limit of about 20% AGN continuum in the same wavelength region due to our larger slit size and extraction region. Further improvement in the optical evidence for an AGN would require a high-quality UV spectrum taken with a narrow slit or a high-quality image, such as is possible with the HST.

5. DISCUSSION

5.1. The Cluster

The X-ray source includes a component from a hot atmosphere of cluster scale with $\beta = 2/3$ and $\theta_{\text{cx}} = 55$ arcsec (section 2.1). Physical parameters for the cluster gas are given in Table 4. The 0.5 - 2.5 keV luminosity is in good agreement with Abell richness class 0 clusters (Briel & Henry 1993), and the extrapolated 2 - 10 keV luminosity of 3.7×10^{42} ergs s $^{-1}$ is consistent with David et al. (1993)'s temperature - luminosity correlation.

Table 2 gives the mean cooling time for gas within θ_{cx} calculated using equations 10 and 25 of Birkinshaw & Worrall (1993). The cooling time within one core radius is comparable to the Hubble time for the best-fit model, suggesting that a strong cluster cooling flow is unlikely. However, there are acceptable fits with small core radii and significant cooling flows. Whereas a β -model profile is quite flat at small radii, a cooling flow would give excess emission of steeper gradient. A strong contribution of such a component of scale-size $\gtrsim 5$ arcsec is ruled out by the excellent fit of the PRF to the November 1995 HRI data (Fig. 3). Moreover, since ROSAT finds compact X-ray emission (section 5.2) of almost ten times the luminosity of the cluster, it is highly unlikely that a cluster cooling flow dominates the central X-ray emission. However, data of higher spatial resolution are needed to place useful constraints on a possible contribution.

Before concluding that the predominant X-ray emission from J2310-437 is associated with an AGN, we should also consider X-ray emission from unusually dense, sub-galaxy, hot gas. For simplicity we characterize the unresolved HRI emission as produced in a sphere of uniform density with a radius of 11.4 kpc, corresponding to a conservative limit of 5 arcsec radius. The two-component thermal fits to the PSPC data (Tanambaum et al. 1997) constrain the temperature of the cooler gas to ~ 0.1 keV, giving a cooling time of $\sim 1.7 \times 10^7$ years and $\sim 6500M_\odot$ per year of cooling gas. We might expect one H α recombination photon to be released per cooling atom, giving a rate of $\sim 2 \times 10^{53}$ H α photons s $^{-1}$. However, our upper limit of 6.0×10^{-16} ergs cm $^{-2}$ s $^{-1}$ for the H α flux (section 4) corresponds to $\lesssim 10^{51}$ H α photons s $^{-1}$. Even assuming that the unresolved HRI emission is associated with the warmer PSPC component, at a temperature of 1 keV, we still estimate a cooling rate of $\sim 600M_\odot$ per year and many more H α photons than allowed by our upper limit. Moreover, in this case we would have the unusual situation of the cooling component having a higher temperature than the gas feeding it. The problem is compounded by the fact that the H α measured from cooling flows is typically 10 to even 1000 times larger than predicted by the simple one photon per recombination argument, implying additional excitation processes (Donahue & Voit 1997). We therefore conclude that it is extremely unlikely that the compact X-rays have a hot-gas origin.

Table 5 compares the minimum internal pressure, P_{min} , for features in the radio source with the pressure from the X-ray

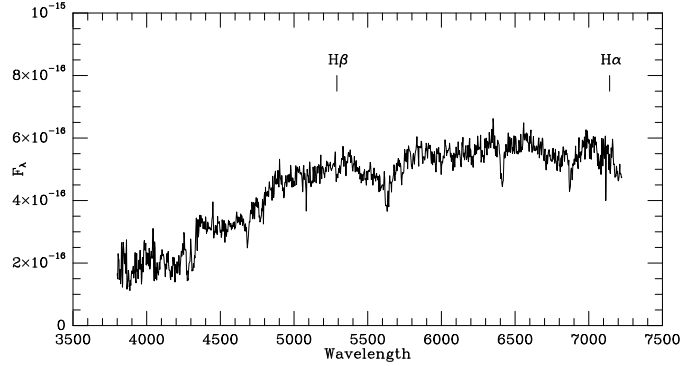


FIG. 6.— Flux-calibrated observed-frame spectrum of the core of J2310-437, obtained with the CTIO 1.5 m telescope. Flux density, in units of $\text{ergs cm}^{-2} \text{s}^{-1} \text{A}^{-1}$, is plotted against wavelength in A . There is no evidence for an AGN in the spectrum from emission lines or the size of the Ca II break (at 4350 A observed frame, 4000 A rest frame). The flux density is lower than in the earlier spectrum of Tucker et al. (1995) due to a different slit size and extraction region.

TABLE 4
PARAMETERS FOR THE CLUSTER X-RAY EMISSION AROUND J2310-437.

Parameter	Value	Reference
Redshift	0.0886	1
Galactic N_H	$1.5 \times 10^{20} \text{ cm}^{-2}$	2
β^a	2/3	3
θ_{cx}^a	55 arcsec	3
B_o^a	$(2.84 \pm 0.49) \times 10^{-6} \text{ PSPC cts s}^{-1} \text{ arcsec}^{-2}$ (0.17-1.8 keV)	3
Total count rate	$0.054 \pm 0.01 \text{ PSPC cts s}^{-1}$ (0.17-1.8 keV)	3
kT , Abundance	1.18 keV, 50% cosmic	4
Central density	$1.9 \times 10^{-3} \text{ cm}^{-3}$	3
$L_{0.1-2.4 \text{ keV}}$	$2.6 \times 10^{43} \text{ ergs s}^{-1}$	3
$L_{0.5-2.4 \text{ keV}}$	$1.8 \times 10^{43} \text{ ergs s}^{-1}$	3

^a For β model of the form $S = B_o(1 + \frac{\theta^2}{\theta_{\text{cx}}^2})^{0.5-3\beta}$

REFERENCES.—(1) Tucker et al. 1995; (2) Tananbaum et al. 1997 based on Heiles & Cleary 1979; (3) this paper; (4) ROSAT PSPC from Tananbaum et al. 1997

emitting cluster gas. We find that the gas is over-pressured with respect to P_{\min} , as is common for kpc-scale structures of low-power radio sources (e.g., Morganti et al. 1988, Böhringer et al. 1993, Trussoni et al. 1997). Possible explanations (e.g., Hardcastle, Worrall & Birkinshaw 1998b) include dynamical effects, where the outer radio structure is expanding, or contributions to the jet pressure from relativistic or thermal (entrained) protons, or clumping. X-ray maps of higher resolution than from the PSPC are required for a more detailed assessment of the relationship between the rather unusual outer radio structure (section 3.3) and the X-ray emitting cluster medium.

5.2. The AGN

5.2.1. Radio morphology and X-ray strength

The most striking features of the radio maps of J2310-437 are

1. the flat-spectrum radio core, seen in the C- and X-band maps;
2. the one-sided, small-scale jet, seen best in the C- and X-band maps; and
3. the two-sided large-scale plumes, seen best in the L-band, low-resolution image.

The immediate inference from (1) is that J2310-437, despite its “normal” optical appearance and line-free optical spectrum, does indeed host an AGN. Much of the interest in studying this object then shifts to attempting to understand what type of AGN we are observing.

The large-scale, two-sided radio morphology of J2310-437 seen in the low-resolution images is reminiscent of the structures of Fanaroff and Riley (1974) type 1 (FR1) radio galaxies – “plumes” of radio emission extending to either side of the bright central part of the source near the radio core, and with no sign of “hot-spots” in the radio lobes. At high resolution the source exhibits a 1-sided jet as often seen in FR1 radio galaxies. The relatively low L-band radio power of the source, $P_{1384} \approx 3.5 \times 10^{31}$ ergs s⁻¹ Hz⁻¹, is also consistent with its classification as an FR1 radio galaxy (Owen & White 1991).

However, the associated X-ray emission, at $l_{1 \text{ keV}} = 1.5 \times 10^{26}$ ergs s⁻¹ Hz⁻¹, is anomalously bright for FR1 radio galaxies; a representative sample of such radio galaxies have $l_{1 \text{ keV}}$ in the range 6×10^{22} to 10^{25} ergs s⁻¹ Hz⁻¹ (Worrall 1997). The core X-ray power of J2310-437, $P_{0.1-2.4 \text{ keV}} \approx 1.7 \times 10^{44}$ ergs s⁻¹, is more similar to that of a BL Lac object. But if we interpret J2310-437 as a BL Lac object embedded in an elliptical galaxy, we must ask

1. Is the radio structure similar to that of other X-ray selected BL Lacs (XBLs)?
2. Why do we not see a classically-bright optical nucleus of BL Lac type?
3. Are there other objects of similar type, largely unrecognized in existing samples of X-ray or radio sources?

While radio-selected BL Lacs are dominated by bright, variable, and polarized radio nuclei, and have featureless optical spectra, XBLs have lower radio powers and are generally found in lower-redshift galaxies (Schwartz et al. 1989). For a sample of 20 XBLs from the HEAO-1 A1 survey, Laurent-Muehleisen

et al. (1993) find an average total radio power $P_{L\text{-band}} \approx 10^{31}$ ergs s⁻¹ Hz⁻¹, an average core/extended L-band emission ratio ≈ 4 , and an average $P_{2 \text{ keV}}/P_{L\text{-band}}$ ratio $\approx 10^{-4}$. In J2310-437, the total radio power ($\approx 3.5 \times 10^{31}$ ergs s⁻¹ Hz⁻¹) lies close to the expected value, the radio core is weak (the core/extended L-band ratio is < 0.25), and the ratio of the X-ray and extended radio powers is low at $\approx 2 \times 10^{-6}$, although not as low as the average value of $\approx 3 \times 10^{-7}$ found by Laurent-Muehleisen et al. (1993) for a sample of FR1 radio galaxies. J2310-437 lies within the range of properties seen for the XBLs, but with radio and X-ray cores which are at the weakest end of the distribution with respect to extended radio power. This may suggest that the core of J2310-437 is less subject to relativistic boosting than an average XBL.

0548-322 is a weak-cored XBL in the HEAO A1 sample; it has been mapped by Antonucci & Ulvestad (1984) and Laurent-Muehleisen et al. (1993). This source has several similarities to J2310-437: $z = 0.0689$, $P_{L\text{-band}} = 8 \times 10^{31}$ ergs s⁻¹ Hz⁻¹, core/extended L-band ratio of 0.2, and $P_{2 \text{ keV}}/P_{L\text{-band}} \approx 4 \times 10^{-6}$. The radio structures and polarization are also similar: 0548-322 shows large-scale radio plumes, extending over more than 150 kpc, and the central structure suggests that a one-sided jet may be present. The linear polarization is ~ 10 per cent in the core and ~ 8 per cent in the extended emission, with a transverse magnetic field in both regions. The optical field of 0548-322 indicates that, like J2310-437, it is embedded in a cluster (in this case Abell richness class 2; Falomo, Pesce & Treves 1995), and the absolute magnitude of the host galaxy of 0548-322 ($M_V = -23.4$) is brighter than J2310-437 ($M_V = -22.67$; Tucker et al. 1995) by a factor similar to the ratio of total radio powers.

The main difference between the two objects is the presence of strong optical continuum in 0548-322, where ~ 50 per cent of the 4200 Å light (observed frame) comes from the AGN (Falomo et al. 1994). This is large, particularly considering the fact that the effective aperture used in the observations was $8'' \times 8''$ and so dilution due to galaxy light should be relatively higher than in our observation of J2310-437 for which $\lesssim 28$ per cent of the 4200 Å light can originate in an AGN. Through its radio and X-ray resemblance to 0548-322, we interpret J2310-437 as a BL Lac embedded in an elliptical galaxy. We now consider in more detail why we do not see an optical nucleus of the BL Lac type, and just how unusual J2310-437 might be.

5.2.2. The weak optical nucleus

Multifrequency parameter values for J2310-437 are summarized in Table 6. Tananbaum et al. (1997) compared earlier limits for two-point spectral indices α_{ro} and α_{ox} with AGN from the work of Stocke et al. (1990), and concluded that although the best overall match was with BL Lac objects, J2310-437 was either an extreme member of the population or distinct. In Tananbaum et al. (1997) the two-point spectral indices are referenced to 5 GHz, 2500 Å and 2 keV in the rest frame, whereas in this paper we reference them to 5 GHz, 4400 Å and 1 keV (rest frame) for better comparison with a larger selection of recent data for BL Lac objects and to reduce extrapolation errors. Our improved upper limit on AGN optical light shifts J2310-437 to a more extreme region in (α_{ro} , α_{ox}) parameter space (Fig. 7). XBLs tend to show some degree of downwards curvature in the two-point spectrum between the radio to X-ray, but J2310-437 is consistent with a single power law of energy index $\alpha_{\text{rx}} = 0.61$. The two point radio to X-ray spectral index for the XBLs is very similar to that for J2310-437; the 123 XBLs in Figure 7 have

TABLE 5
MINIMUM PRESSURE IN L-BAND RADIO FEATURES AND X-RAY GAS PRESSURE.

θ^a (arcsec)	pa ^a (degs)	FWHM (sq arcsec)	B_{eq}^b (μGauss)	P_{min}^b (dynes cm ⁻²)	P_{gas}^c (dynes cm ⁻²)
40	130	31×14	3.4	3.1×10^{-13}	5.2×10^{-12}
40	355	25×14	3.9	4.0×10^{-13}	5.2×10^{-12}
75	15	43×37	1.8	8.6×10^{-14}	2.5×10^{-12}

^aAngular distance and position angle of feature from the radio core

^bEquipartition magnetic field and minimum pressure in radio feature calculated assuming an electron spectral index of 2.6 extending from 3×10^7 to 2×10^{11} eV, a plasma filling-factor of unity, and no protons.

^cGas pressure using cluster parameters from Table 4

a mean α_{rx} of 0.60 ± 0.01 and a median of 0.6 (this compares with steeper average values of 0.86 ± 0.08 for a complete sample of radio-selected BL Lac objects [Sambruna, Maraschi & Urry 1996] and ≈ 0.85 for the cores of low-power radio galaxies [Worrall 1997], possibly because of the way the objects are selected). So, J2310-437 is not unusual compared with XBLs in its ratio of core X-ray to radio emission, but it is extreme in emitting so little optical continuum that a broad-band spectral break is not required.

Data for four sources with multifrequency spectra that resemble J2310-437, most particularly in having weak or undetected optical continuum coupled with similar X-ray to radio ratios, are compiled in Table 7 and plotted in Figure 7. In addition, eight of the sources from the RASS-Green Bank (RGB) XBL sample have seemingly normal elliptical galaxy spectra and are treated as candidate XBLs by Laurent-Muehleisen et al. (1998); they are plotted as limits in Figure 7. Sources with limits share J2310-437's consistency with a single-component power law from the radio to X-ray, but none suggests it as convincingly as J2310-437 itself. Moreover, for J2310-437 a hot-gas origin for the compact X-ray component is extremely unlikely (section 5.1) whereas it remains a possibility for the eight RGB sources (Laurent-Muehleisen et al. 1998), and indeed for similar candidates reported earlier by Brinkmann, Siebert & Boller (1994) and Moran et al. (1996). It will become clear whether or not objects like J2310-437 are truly common or rare through further optical, radio and X-ray follow-up of AGN selected from radio and X-ray surveys (e.g., Laurent-Muehleisen et al. 1998, Caccianiga & Maccacaro 1997).

5.2.3. A photon-starved jet?

Since a single power law connecting the radio and X-ray cores runs a factor of about 2 below the optical upper limit, it is possible to interpret all of this emission as arising from a single region of synchrotron-emitting plasma, where the flat radio spectrum is attributed to a series of self-absorbed components and the optically-thin synchrotron spectral index is $\alpha_s = 0.61$. Assuming Galactic N_H , the best-fit power-law spectral index to the PSPC X-ray emission of 1.43 (Tananbaum et al. 1997) is steeper than α_s ; fixing the X-ray spectral index at 0.61 gives

$\chi^2 = 29$ for a fit to the PSPC spectral data as compared with a minimum χ^2 of 18 for 28 degrees of freedom. This result may suggest that an energy-loss break in the electron spectrum is showing up in the X-ray emission. However, the quality of the data and the complicated mixture of non-thermal and thermal emission in the PSPC means that a definitive result on the shape of the non-thermal X-ray spectrum awaits X-ray data of higher spatial and spectral resolution such as those which could be obtained with AXAF.

Using a computer code developed for the work of Hardcastle, Birkinshaw & Worrall (1998a), we model the nuclear source as a spherical emitting region in which the magnetic field and electron energy densities are in equipartition. Assuming negligible bulk relativistic motion, we can place a lower limit to the radius of the emitting region of 0.2 pc; for smaller sizes the synchrotron self-absorption cut-off frequency would be above 2 GHz. For a radius of 0.2 pc the equipartition magnetic field, B_{eq} , is ≈ 0.07 Gauss, and the single-component electron spectrum must span at least the range $E_{\text{min}} \sim 5 \times 10^7$ to $E_{\text{max}} \sim 10^{12}$ eV to give radiation at ~ 2 GHz and ~ 1 keV. The self-Compton contribution to the X-ray emission is negligible, at $\lesssim 0.1\%$. For larger objects, B_{eq} scales as $(0.2\text{pc}/r)^{6/7}$ and $E_{\text{min,max}}$ scale as $(r/0.2\text{pc})^{3/7}$.

We argued in section 5.2.1 that, since J2310-437's core is relatively weak compared with its extended (isotropic) radio emission, relativistic boosting along the line of sight is likely to be small compared with most BL Lac objects. Relativistic boosting is quantified by the bulk relativistic Doppler factor, δ , which is given by $1/\gamma(1-\beta\cos\theta)$, where γ is the Lorentz factor, β is the velocity as a fraction of the speed of light, and θ is the angle to the line of sight. For a steady jet of optically-thin spectral index α_s and jet to counter-jet ratio R , $\beta\cos\theta = [(R^{2+\alpha_s} - 1)/(R^{2+\alpha_s} + 1)]$ (Scheuer & Readhead 1979; Begelman, Blandford & Rees 1984). Unified models of BL Lacs and radio galaxies with low core to isotropic radio ratios suggest $\theta \gtrsim 30^\circ$ (Padovani & Urry 1990). Our measurements of R (section 3.3) then suggest that $\delta < 2$.

If the AGN in J2310-437 is BL Lac-like, with a relatively large orientation to the line of sight, we have to consider why the X-ray emission is so bright (compared with an FR1 galaxy

TABLE 6
PARAMETERS FOR THE AGN IN J2310-437.

Parameter	Value	Reference
Redshift	0.0886	1
Galactic N_H	$1.5 \times 10^{20} \text{ cm}^{-2}$	2
α_r for radio core	~ 0	3
l_5 GHz for radio core	$(7.0 \pm 0.1) \times 10^{30} \text{ ergs s}^{-1} \text{ Hz}^{-1}$	3
$f_{4400 \text{ \AA}}$	$< 32 \text{ } \mu\text{Jy}$	3
$l_{4400 \text{ \AA}}$ ($\nu = 6.82 \times 10^{14} \text{ Hz}$)	$\leq 1.3 \times 10^{28} \text{ ergs s}^{-1} \text{ Hz}^{-1}$	3
X-ray count rate	$0.086 \pm 0.004 \text{ HRI cts s}^{-1}$	3
f_1 keV	$0.4 \pm 0.04 \text{ } \mu\text{Jy}$	3
α_x	1.43	4
l_1 keV ($\nu = 2.4 \times 10^{17} \text{ Hz}$)	$1.5 \times 10^{26} \text{ ergs s}^{-1} \text{ Hz}^{-1}$	3
$L_{0.1-2.4 \text{ keV}}$	$1.7 \times 10^{44} \text{ ergs s}^{-1}$	3
$\alpha_{\text{ox}}^{\text{a}}$	≤ 0.76	3
$\alpha_{\text{ro}}^{\text{b}}$	≥ 0.53	3
$\alpha_{\text{rx}}^{\text{c}}$	0.61	3

$$^{\text{a}}\alpha_{\text{ox}} = \log(l_{4400 \text{ \AA}}/l_1 \text{ keV}) / 2.5465$$

$$^{\text{b}}\alpha_{\text{ro}} = \log(l_5 \text{ GHz}/l_{4400 \text{ \AA}}) / 5.135$$

$$^{\text{c}}\alpha_{\text{rx}} = \log(l_5 \text{ GHz}/l_1 \text{ keV}) / 7.68$$

REFERENCES.—(1) Tucker et al. 1995; (2) Tananbaum et al. 1997 based on Heiles & Cleary 1979; (3) this paper; (4) ROSAT PSPC from Tananbaum et al. 1997

NOTE.—Flux densities relate to the observed frame. Luminosities are for the rest frame. The error in the X-ray flux density incorporates uncertainties in the amount of cluster emission but does not include spectral-shape uncertainties.

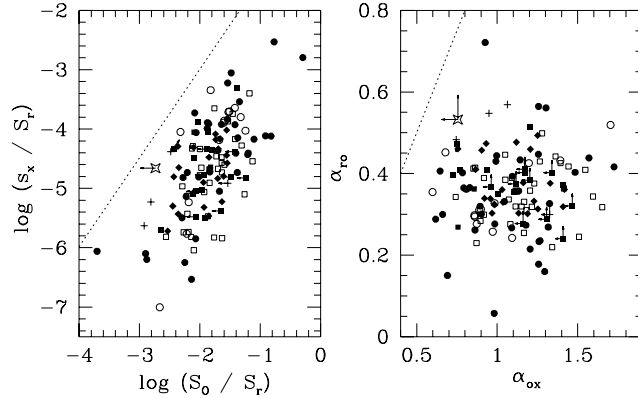


FIG. 7.— Data for J2310-437 from Table 6 (star) and sources from Table 7 (crosses) are plotted with those for the 53 RGB XBLs (including those with low Ca II contrast) from Laurent-Muehleisen et al. (1998; squares), the complete EMSS XBL sample of 22 sources from Morris et al. (1991; diamonds) and the complete N-1ES sample of 48 XBLs from Perlman et al. (1996a; circles). Open symbols show XBLs with no measured redshift. The left plot shows logarithmically the 1 keV X-ray (S_x) vs 4400 Å optical (S_o) flux density, both normalized by the 5 GHz radio flux density (S_r). All flux densities are corrected to the rest frame. The median sample redshifts of 0.13 (RGB) and 0.15 (N 1ES) are used for sources without a redshift. K-corrections for the XBLs use $\alpha_r = 0$, $\alpha_o = 1.0$, and $\alpha_x = 1.2$ (RBL) or 1.35 (N-1ES). X-ray fluxes and K-corrections for the EMSS sample are computed from the ROSAT spectra presented by Perlman et al. (1996b). Optical flux densities are computed assuming the 4400 Å flux density of a zero magnitude object is $10^{6.65}$ mJy for O-band magnitudes for the RGB and N-1ES samples, and $10^{6.463}$ mJy for V-band magnitudes for the EMSS sample. The right hand plot shows the same data in terms of α_{ro} vs α_{ox} , where these parameters are as defined in Table 6. The dashed line on both plots is the locus of sources with a single spectral slope through the radio, optical and X-ray. J2310-437 is an outlier compared with XBL populations and could lie on this locus.

TABLE 7

PARAMETERS FOR OPTICALLY DEFICIENT NUCLEI POSSIBLY SIMILAR TO J2310-437.

Name	z	$f_{1 \text{ keV}} (\mu\text{Jy})$	$\log L_{rx} (\text{ergs s}^{-1})$	α_{ro}	α_{ox}	α_{rx}	references
3C 264	0.0215	0.45	43.37	0.57	1.06	0.73	1,2,3
E 0336-248	0.251	0.45	45.12	≤ 0.48	0.75	≤ 0.57	4
26W20	0.054	0.63	44.75	≥ 0.3	≤ 1.33	0.64	5, 6
PKS 2316-423	0.0549	0.85	44.27	≥ 0.55	0.95	0.68	7, 8, 6
J 2310-437	0.0886	0.4	44.12	≥ 0.53	≤ 0.76	0.61	9

REFERENCES.—(1) Giovannini et al. 1990; (2) Crane et al. 1993; (3) Tananbaum et al. 1997; (4) Halpern et al. 1997; (5) Harris et al. 1984; (6) Silverman et al. 1998; (7) Wright et al. 1997; (8) Crawford & Fabian 1994; (9) this paper

NOTE.— L_{rx} is the luminosity from 5 GHz to 1 keV in the source frame assuming α_{ro} and α_{ox} . For $\alpha_{ox} < 1$ the X-ray contribution dominates and quoted luminosities extend only to 1 keV. Parameters for 3C 264 differ from those in Tananbaum et al. (1997) because of the redefinition of reference frequencies for the two-point spectral indices and use here of an improved (lower) radio core flux density of 200 mJy. The radio flux density for E 0336-248 is treated as an upper limit due to lack of high spatial resolution mapping. For 26W20 the X-ray flux density is from the average of the ROSAT measurements, and the optical is dominated by galaxy light; no continuum separation has been attempted in references 5 and 6. For PKS 2316-423 the higher spatial resolution mapping in reference 7 updates information in reference 8. The claimed similarity to J2310-437 is in the last reference for each source.

nucleus), and why there is no evidence of optical continuum or line emission. Ulrich (1989) has shown that a sample of radio galaxies selected from the B2 radio survey is particularly well matched to BL Lac objects in extended (isotropic) radio emission and galaxy magnitude. In Figure 8 we compare our upper limit to the emission-line luminosity of J2310-437 with measurements for B2 galaxies from Morganti, Ulrich & Tadhunter (1992). The plot shows core radio power on the abscissa since a correlation with line luminosity is claimed for larger samples of FR1 radio galaxies (Baum, Zirbel & O’Dea 1995). We find that radio galaxies with the same core radio power as J2310-437 generally have lines detectable at levels higher than the upper limit for J2310-437. If we assume that the line emission in FR1 radio galaxies is due to photoionization (but see Baum et al. 1995), then we might expect J2310-437’s line emission to be enhanced relative to galaxies of the same radio-core power since its ratio of X-ray to radio strength is higher ($\alpha_{\text{rx}} = 0.61$) than for a typical FR1 radio galaxy ($\alpha_{\text{rx}} = 0.85$). Perhaps this indicates that line-emitting clouds in J2310-437 are indeed weak or absent. Baum et al. (1995) argue that the FR1/BL Lac population is deficient in isotropic radiant optical/UV energy with respect to higher-power radio galaxies, possibly due to a lower accretion rate. J2310-437 may show an extreme ratio of bulk kinetic energy in the jet to radiant isotropic energy close to the central AGN.

The possibility that J2310-437 exhibits a single-component synchrotron spectrum from the radio to the X-ray distinguishes it from BL Lac objects which show strong curvature and relatively more optical emission. Landau et al. (1986) found the radio to X-ray spectrum of a BL Lac object was well described by a parabola. A remarkable correlation between the half-width of the parabola and bolometric luminosity of the source (Jones, Rudnick & Landau 1986), in the sense of less luminous sources displaying an overall flatter spectrum, led these authors to suggest that the underlying physical quantities determining the spectra from such sources are limited in number. Worrall (1989) showed the X-ray emission in radio-selected BL Lac objects was consistent with an extrapolation of the parabola, but that a spectral discrepancy hinted at a possible admixture of flat-spectrum Compton emission. In Figure 9 we compare J2310-437 with the objects from Figure 7 in plotting the size of the break in spectral index between α_{ro} and α_{ox} against the logarithm of the sum of the two-point radio (5 GHz) to optical (4400 Å) and optical to X-ray (1 keV) luminosity. The abscissa is a measure of the bolometric luminosity whereas the ordinate is a measure of the degree of curvature in the spectrum. A correlation of greater curvature with larger luminosity is not apparent in this figure, but the extreme position of J2310-437 compared with other XBLs is again obvious.

The work of Landau et al. (1986) has been extended by Sambruna et al. (1996), who fit parabolas to the spectra of BL Lac objects and core-dominated quasars and argue that lower-power sources have higher peak frequencies in νl_{ν} . In J2310-437 we have found that the break frequency may be within or above the X-ray band. Since the lack of line emission in J2310-437 may indicate an overall shortage of optical and UV photons external to the jet in the central regions of the source, the source’s properties are consistent with the intensity of external photons governing the electron spectral break through Compton cooling: a higher external photon density produces a lower-energy electron spectral break (Ghisellini 1997). In J2310-437 the external photon density may be sufficiently low as to allow an unbroken synchrotron spectrum from the radio to the X-ray.

We have interpreted the AGN in J2310-437 as a jet in which the electron population produces X-ray synchrotron radiation more effectively than in most BL Lac objects and FR1 radio galaxies. It is important to ascertain how common or rare such sources are, as discussed in section 5.2.2. In particular, the discovery of X-ray galaxies/AGN with optical continuum deficits, no emission lines, but no core radio emission (i.e., radio-quiet versions of J2310-437) may point to a completely different interpretation. Such a population may have been found by Griffiths et al. (1995), in their so-called ‘passive X-ray galaxies’, although here the authors favor attributing the strong X-ray emission to a hot coronal halo, possibly in the early stages of a cooling flow, which is an unlikely explanation for J2310-437.

6. CONCLUSIONS

The ROSAT HRI X-ray data and ATCA radio imaging and polarization measurements confirm the presence of an AGN in the elliptical galaxy J2310-437. The radio properties are reminiscent of an FR1 radio galaxy, even in the sense that the cluster-scale X-ray emitting medium around J2310-437 is over-pressured with respect to the minimum pressure in the radio structures. There may be a cooling flow associated with the cluster gas, but the central X-ray emission from this would provide only a small contribution to the compact X-ray source.

The radio data, including the strength of the core relative to the extended (isotropic) emission, suggest an ordinary FR1 radio galaxy with its jet at $\gtrsim 30^\circ$ to the line of sight. However, the relative strength of the X-ray emission suggests we are observing a low-power BL Lac-type nucleus, and J2310-437’s radio and X-ray properties are not entirely without precedent for an X-ray selected BL Lac object. What then makes the source extreme is a lack of the expected level of optical continuum. Whereas the multiwavelength spectra of BL Lac objects fit parabolas between the radio and X-ray, in J2310-437 a single power law connecting the radio and X-ray runs a factor of about 2 below the optical upper limit, and it is possible to interpret all of the emission as arising from a single region of synchrotron-emitting plasma. J2310-437 is the most extreme such source known.

Low-power sources are normally the most deficient in central isotropic radiant optical/UV energy with respect to jet power, a feature which Baum et al. (1995) attribute to low accretion rate. Moreover, it is argued that the lowest-power sources have the highest (jet) peak frequencies in νl_{ν} (Sambruna et al. 1996). J2310-437 may be interpreted as an extreme low-power source in which a single synchrotron component extends to, and peaks in, the X-ray band, at which point the PSPC data suggest spectral steepening may occur. J2310-437’s low isotropic optical/UV radiation is consistent with the idea that the intensity of external photons governs the electron spectral break through Compton cooling (Ghisellini 1997): in this source the external photon density would be too low to produce a spectral break below the X-ray. Such an explanation for the AGN in J2310-437 would be challenged by the discovery of ‘radio-quiet’ versions of the source.

We thank Günther Hasinger for discussions concerning ROSAT’s aspect determination errors, and John Silverman and Dan Harris for providing preliminary versions of IRAF scripts being developed to help correct for such errors. Martin Hardcastle provided software used to calculate physical parameters for the radio emission. RAR acknowledges the excellent ob-

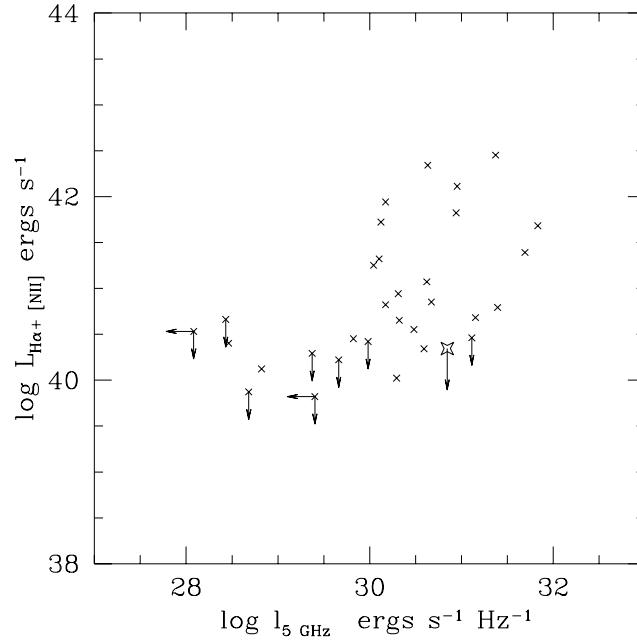


FIG. 8.— $H\alpha + [N II]$ luminosity versus 5 GHz core radio power for the B2-selected sample of low-power radio galaxies (crosses) from Morganti et al. (1992; adjusted to $H_o = 50 \text{ km s}^{-1} \text{ Mpc}^{-1}$ used in this paper) and J2310-437 (star). The radio to X-ray spectral index of 0.61 for J2310-437 is flatter than for the B2 radio galaxies (average value roughly 0.85) and so the factor of ~ 70 times larger X-ray luminosity with respect to a radio galaxy of the same radio core strength makes it surprising that J2310-437 does not have lines of a detectable strength.

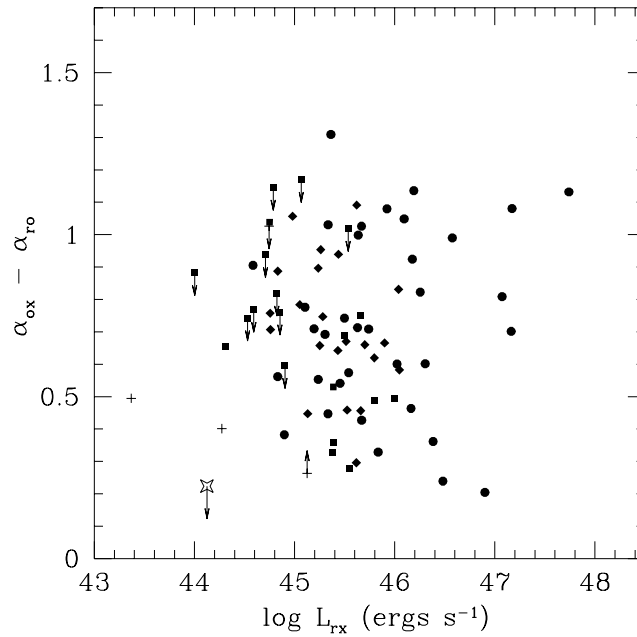


FIG. 9.— Size of break in spectral index between α_{ro} and α_{ox} plotted against the logarithm of the sum of the two-point radio (5 GHz) to optical (4400 Å) and optical to X-ray (1 keV) luminosities for objects from Figure 7 with measured redshifts. J2310-437 (star) is at the low end of the XBL luminosity range and shows little or no spectral curvature.

server support provided by the staff at CTIO. DMW and MB thank the following ‘duty officers’ and ‘friends’ for help before and during the ATCA observing run: Vince McIntyre, John Reynolds, Tasso Tzioumis and Bob Sault. The Australia Telescope is funded by the Commonwealth of Australia for opera-

tion as a National Facility managed by CSIRO. We acknowledge support from NASA grants NAG 5-3205 and NAG 5-1882. RAR’s CTIO observing was supported by travel grant NSF AST 9315074, and travel support for DMW and MB to observe with the ATCA was provided by the PPARC.

APPENDIX

EFFECT OF ROSAT ASPECT CORRECTION ERRORS ON THE J2310-437 HRI DATA

David et al. (1996) illustrate the effects of residual errors in the ROSAT aspect solution by showing HRI images of 6 stellar sources measured at small off-axis angles. They point out that the surface brightness at radii between 5 and 8 arcsec from the center of the images can exhibit some asymmetry; the feature is randomly oriented and cannot be predicted through knowledge of the roll angle. In particular, a source observed at different epochs, with different roll angles, may be affected differently and unpredictably.

The problem responsible for this behavior has been described by G. Hasinger in private discussions during 1997. It is believed that there are gain changes between neighboring 1 arcmin² pixels in the aspect camera, with possibly as many as 20-30% of the pixels returning inaccurate centroids. The full aspect-camera data are not returned in the telemetry stream, only the computed centroids. Problematic pixels may then be used for aspect corrections for some phases of the 402 sec spacecraft wobble which, of amplitude about ± 3 arcmin, is employed when the HRI is in focus in order to average out any changes in quantum efficiency over the detector. Depending on the roll angle and the positions of aspect stars, some observations are entirely free from errors, although which observations are unaffected cannot be predicted in advance, nor after the fact (except based on the quality of the X-ray images).

Since the relative wobble phase is given by the spacecraft clock, which is rarely reset, Hasinger’s suggested procedure for improving the aspect errors in a given data set is to fold the data on the wobble period and divide into some number of phase bins. A centroid should be found for data in the resulting set of time intervals for each phase bin in turn. A shift should then be applied so that these centroids are aligned. Only data for the same roll angle (which changes in increments of multiples of 1 degree) should be analyzed together. The amplitude of the wobble relative to the size of pixels in the aspect camera implies that at least 10 phase bins should be used. Morse (1994) showed empirically that for a bright stellar source the spread of counts sharpened significantly when sub-images defined using detector coordinates as an indicator of satellite wobble-position were selected and stacked to a common centroid. Morse suggests that for an HRI target of 0.35 cts/s (cf 0.1 cts/s for J2310-437), 20 to 30 bins should provide a reasonable trade-off between fineness of phase grid and adequate counts for determination of good centroids.

The 1996 observations of J2310-437 stretched over more than a month and spanned 4 roll angles in a 20 degree band; a severe disadvantage. Had there been, within about 6 arcmin of J2310-437, a bright X-ray source identified with a point-like emitter, we could have used the radial distribution of its counts as representative of the PRF for the observation; unfortunately no such source is present. So, assisted by preliminary versions of IRAF scripts being written by John Silverman and Dan Harris for distribution by the US-RSDC/SAO, we attempted the ‘dewobble’ procedure described above on the 1996 data of J2310-437. Rather than analyze the data-set as one, we broke it into 5 time intervals, each of constant nominal roll angle. For the sake of centroid accuracy it then seemed unreasonable to divide the data into more than 10 phase bins. We smoothed and contoured each of the separate 50 images before re-stacking. In only about half the cases did this produce an image which was more radially symmetric than the composite, and other cases were significantly more elongated. This suggests that 10 phase bins are too few, but the relative weakness of the source coupled with the several changes in roll angle makes it a poor candidate for finer binning. Thus we are not able to correct for the spread in the 1996 data introduced by residual aspect errors.

J2310-437 does, however, present a particularly interesting case in that the 1995 data fit the nominal PRF so well. This fact, coupled with the similar flux measured in 1996, leads us to believe that attitude smearing must be the cause of elongation in the 1996 data. It is then useful to characterize the amount of smearing by fitting a beta model convolved with the nominal PRF to the 1996 data; the parameters found for the β model are then of a size which we would not necessarily believe as real if determined for some other data set. We have broken the data into 6 time intervals, where each spans no more than 3 days. For each we have extracted a radial profile, using the method described for the 1995 data in the main body of the text. The net counts range between about 100 and 1000 counts, depending on segment. χ^2 vs core radius is plotted in Figure A10 for four different values of β . The plots indicate, for example, that a data set which fits a β model of $\beta = 2/3$ and core radius $\lesssim 3$ arcsec, or $\beta = 0.9$ and core radius $\lesssim 5$ arcsec, are within the regime where aspect smearing could be responsible for the results.

REFERENCES

- Antonucci, R.R.J. & Ulvestad, J.S. 1984, *Nature*, 308, 617
 Baum, S.A., Zirbel, E.L. & O’Dea, C.P. 1995, *ApJ*, 451, 88
 Begelman, M.C., Blandford, R.D. & Rees, M.J. 1984, *Rev. Mod. Phys.*, 56, 255
 Böhringer, H., Voges, W., Fabian, A.C., Edge, A.C., Neumann, D.M. 1993, *MNRAS*, 264, L25
 Birkinshaw, M. 1994, in *Astronomical Data Analysis Software and Systems III*, ASP Conference Series Volume 61, eds. D.R. Crabtree, R.J. Hanisch & J. Barnes, 249.
 Birkinshaw, M. & Worrall, D.M. 1993, *ApJ*, 412, 568
 Briel, U.G. & Henry, J.P. 1993, *A&A*, 278, 379
 Brinkmann, W., Siebert, J. & Boller, T. 1994, *A&A*, 281, 355
 Brissenden, R.J.V., Tuohy, I.R., Remillard, R.A., Schwartz, D.A. & Hertz, P.L. 1990, *ApJ*, 350, 578
 Caccianiga, A. & Maccacaro, T. 1997, *AJ*, 114, 2350
 Condon, J.J., Griffith, M.R. & Wright, A.E. 1993, *AJ*, 106, 1095
 Crane, P. et al. 1993, *ApJ*, 402, L37
 Crawford, C.S. & Fabian, A.C. 1994, *MNRAS*, 266, 669
 David, L.P., Harnden, F.R., Kearns, K.E. & Zombeck, M.V. 1996, *The ROSAT High Resolution Imager Calibration Report*, US-RSDC/SAO; available from http://hea-www.harvard.edu/rosat/rsdc_www/hricalrep.html
 David, L.P., Slyz, A., Jones, C., Forman, W., Vrtilek, S.D. & Arnaud, K.A. 1993, *ApJ*, 412, 479
 Donahue, M. & Voit, G.M. 1997, in *Galactic and Cluster Cooling Flows*, ed. N. Soker, (ASP conference Series Vol 115), 48.

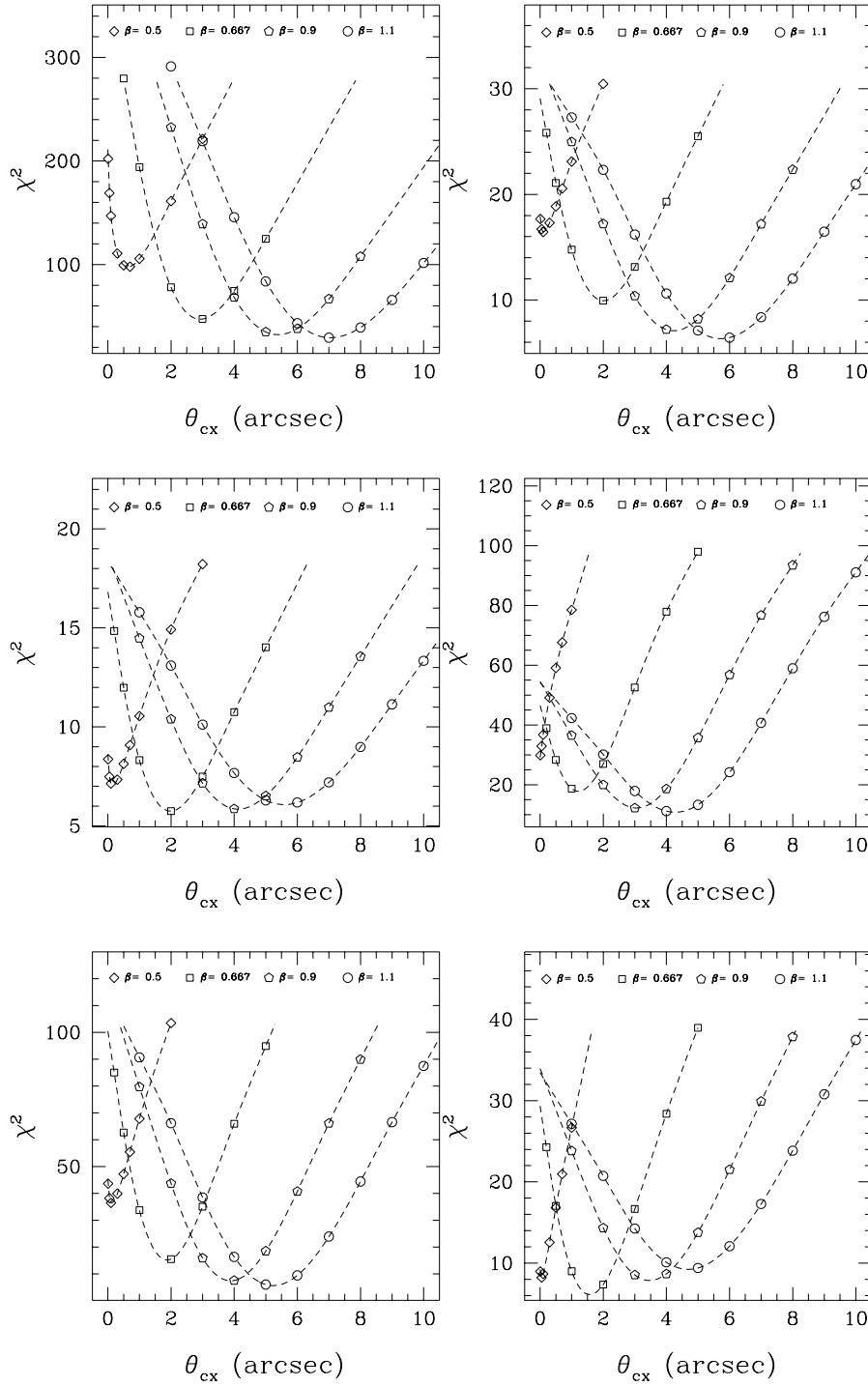


FIG. A10.— Results of fitting a beta model convolved with the nominal PRF to six subsections of the 1996 HRI data, each of duration no more than 3 days. Each fit has 14 degrees of freedom. The subsections of data are not of equal length, and the net counts in the profiles, clockwise starting with the top-left figure, are 958, 118, 295, 200, 418, and 90. Since the 1995 HRI data indicate that the source in reality should be unresolved to the HRI, these fits quantify aspect smearing in terms of β -model parameter values.

- Dressler, A. & Shectman, S.A. 1987, *AJ*, 94, 899
- Falomo, R., Scarpa, R., Bersanelli, M. 1994, *ApJS*, 93, 125
- Falomo, R., Pesce, J.E. & Treves, A. 1995, *ApJ*, 438, L9
- Fanaroff, B.L. & Riley, J.M. 1974, *MNRAS*, 167, 31p
- Ghisellini, G. 1997, in *Relativistic Jets in AGNs*, ed. M. Ostrowski, M. Sikora, G. Madjeski & M. Begelman (Astronomical Observatory of the Jagiellonian University, Krakow), 262 (astro-ph/9706216)
- Giovannini, G., Feretti, L. & Comoretto, G. 1990, *ApJ*, 358, 159
- Griffith, M.R. & Wright, A.E. 1993, *AJ*, 105, 1666
- Griffiths, R.E., Georgantopoulos, I., Boyle, B.J., Stewart, G.C., Shanks, T. & Della Ceca, R. 1995, *MNRAS*, 275, 77
- Halpern, J.P., Eracleous, M. & Forster, K. 1997, *AJ*, 114, 1736
- Hardcastle, M.J., Birkinshaw, M. & Worrall, D.M. 1998a, *MNRAS*, 294, 615
- Hardcastle, M.J., Worrall, D.M. & Birkinshaw, M. 1998b, *MNRAS*, 296, 1098
- Harris, D.E., Costain, C.H. & Dewdney, P.E. 1984, *ApJ*, 280, 532
- Heiles, C. & Cleary, M.N. 1979, *Australian J. Phys. Suppl.* 47, 1
- Jones, T.W., Rudnick, L. & Landau, R. 1986, in *Continuum Emission in Active Galactic Nuclei*, ed. M.L. Sitko (Tucson: KPNO/NOAO), 122
- Landau, R. et al. 1986, *ApJ*, 308, 78
- Laurent-Muehleisen, S.A., Kollgaard, R.I., Moellenbrock & Feigelson, E.D. 1993, *AJ*, 106, 875
- Laurent-Muehleisen, S.A., Kollgaard, R.I., Ciardullo, R., Feigelson, E.D., Brinkmann, W. & Siebert, J. 1997, *ApJS*, in press (astro-ph/9711268)
- Marchã, M.J.M., Browne, I.W.A., Impey, C.D. & Smith P.S. 1996, *MNRAS*, 281, 425
- Moran, E.C., Helfand, D.J., Becker, R.H. & White, R.L. 1996, *ApJ*, 461, 127
- Morganti, R., Fanti, R., Gioia, I.M., Harris, D.E., Parma, P. & de Ruiter, H. 1988, *A&A*, 189, 11
- Morganti, R., Ulrich, M.-H. & Tadhunter, C.N. 1992, *MNRAS*, 254, 546
- Morris, S.L., Stocke, J.T., Gioia, I.M., Schild, R.E., Wolter, A., Maccacaro, T. & Della Ceca, R. 1991, *ApJ*, 380, 49
- Morse, J.A. 1994, *PASP*, 106, 675
- Owen, F.N. & White, R.A. 1991, *MNRAS*, 249, 164
- Padovani, P. & Urry, C.M. 1990, *ApJ*, 356, 75
- Perlman, E.S., et al. 1996a, *ApJS*, 104, 251
- Perlman, E.S., Stocke, J.T., Wang, Q.D. & Morris, S.L. 1996b, *ApJ*, 456, 451
- Pinkey, J., Burns, J.O. & Hill, J.M. 1994, *AJ*, 108, 2031
- Sambruna, R.M., Maraschi, L. & Urry, C.M. 1996, *ApJ*, 463, 444
- Sarazin, C.L. 1986, *Rev. Mod. Phys.*, 58, 1
- Scheuer, P.A.G. & Readhead, A.C.S. 1979, *Nature*, 277, 182
- Schwartz, D.A., Brissenden, R.J.V., Tuohy, I.R., Feigelson, E.D., Hertz, P.L. & Remillard, R.A., 1989, in *BL Lac Objects*, ed. L. Maraschi, T. Maccacaro, M-H. Ulrich (Springer: Berlin), p. 209
- Silverman, J.D., Harris, D.E. & Junor, W. 1998, *A&A*, 335, 443
- Stocke, J.T. et al. 1990, *ApJ*, 348, 141
- Tananbaum, H., Tucker, W.H., Prestwich, A. & Remillard, R.A. 1997, *ApJ*, 476, 83
- Trussoni, E., Massaglia, S., Ferrari, R., Fanti, R., Feretti, L., Parma, P. & Brinkmann, W. 1997, *A&A*, 327, 27
- Tucker, W.H., Tananbaum, H. & Remillard, R.A. 1995, *ApJ*, 444, 532
- Ulrich, M.-H. 1989, in *BL Lac Objects*, ed. L. Maraschi, T. Maccacaro, M-H. Ulrich (Springer: Berlin), p. 45
- Worrall, D.M. 1989, in *BL Lac Objects*, ed. L. Maraschi, T. Maccacaro, M-H. Ulrich (Springer: Berlin), p. 305
- Worrall, D.M. & Birkinshaw, M. 1994, *ApJ*, 427, 134
- Worrall D.M. 1997, in *Relativistic Jets in AGNs*, ed. M. Ostrowski, M. Sikora, G. Madjeski & M. Begelman (Astronomical Observatory of the Jagiellonian University, Krakow), 20 (astro-ph/9709165)
- Wright, A.E. et al. 1997, *Accurate positions, fluxes and structure for 6603 southern radio sources*, available from ftp.atnf.csiro.au, under the directory /pub/data/pmn/CA